JOURNAL OF MATERIALS SCIENCE 27 (1992) 3667–3679

Experimental study of quantitative phase characterization in duplex stainless steels by potentiostatic etching

J. H. POTGIETER, L. M. MATTHEWS, P. DE VISSER
Physical Metallurgy Division, Mintek, Private Bag X3015, Randburg 2125, Republic of South Africa

An investigation into the potentiostatic etching of one commercial and several experimental duplex stainless steels is described. Although no relationship could be deduced from potentiodynamic responses with regard to suitable etching potentials, several useful results were nevertheless obtained from the work. Etching potentials that give the best results for the different types of alloy were experimentally determined, and it was also established that the shortest possible etching time yields the best results. Problems experienced with the potentiostatic etching of copper-containing manganese duplex stainless steels were identified and solved by use of a tint-etch procedure.

1. Introduction

The application of image analysers to measure various microstructural parameters requires the selective detection of the phases of interest. Metallographic etching techniques are particularly suitable for this purpose, provided that the etching technique utilized accurately delineates the phase or constituent of interest.

The major drawback of conventional metallographic etching is that it is difficult to obtain sufficient black and white contrast between the phases of interest. This is a particular problem in distinguishing between the austenite and ferrite phases in duplex stainless steels, even when stain-etching techniques are used.

Potentiostatic etching has been found to give excellent contrast and a consistent colour density for determinations by image analysis, especially for commercial duplex stainless steels [1]. During potentiostatic etching, an interference film is formed by an electrochemical reaction between the etchant and the specimen [2]. During etching, whether a potentiostatic or tint-etch procedure is used, a thin, transparent, adherent layer is formed, the thickness of which varies from one constituent or phase to the next. When stainless steels are tint-etched, the anodic constituents such as ferrite, austenite and martensite are coloured, whereas the cathodic ones such as carbides and nitrides are unaffected and appear bright. A variety of hues can be produced in the anodic constituents as a result of differences in crystallographic orientation. The colours are observed as a result of interference phenomena caused by the thickness of the thin film.

Many useful properties of duplex stainless steels depend strongly on the ferrite-to-austenite ratio, and consequently the strict microstructural control of both cast and wrought duplex stainless steels is of paramount importance to producers and end-users. An accurate, fast and reliable method for measurement of the ferrite or austenite content of a duplex stainless steel is therefore critical.

Various etchants that produce colour differences have been used to distinguish between austenite and ferrite phases in duplex stainless steels. Etchants used to colour the ferrite phase include Murakami's reagent [3], Beraha's tint-etch, electrolytic 20 % NaOH, 56 % KOH and 60 % HNO_3 [4]; Groesbeck's reagent [5] is often used for colouring the austenite phase. Kallings reagent [6] is also used, very often to delineate grain boundaries. However, in previous experiments carried out in this laboratory with various etching solutions, it was found that a 10 N NaOH (40 %) solution is the most successful etchant for use with commercial duplex stainless steels [7] to determine austenite and ferrite phase contents. It was also shown previously [8] that etching in 10 N NaOH yields results that are in excellent agreement with those obtained by X-ray diffraction (XRD), except for very high-chromium (more than 30 %) duplex stainless steels, where preferred orientations influenced the XRD accuracy.

In potentiostatic etching the interference film is formed by an electrochemical reaction between the etchant (electrolyte) and the specimen. The effect of the etchant depends on the composition of the specimen, and in a duplex alloy where the austenite and ferrite phases are electrochemically different this will result in the formation of a transparent layer the thickness of which will vary from one phase to the next. A densitometry determination of the consequent colour differences between the different phases will produce a histogram of reflectance values such as the one shown in Fig. 1. The more prominent phase with lower reflectivity and thus greater contrast can be used for

0022–2461

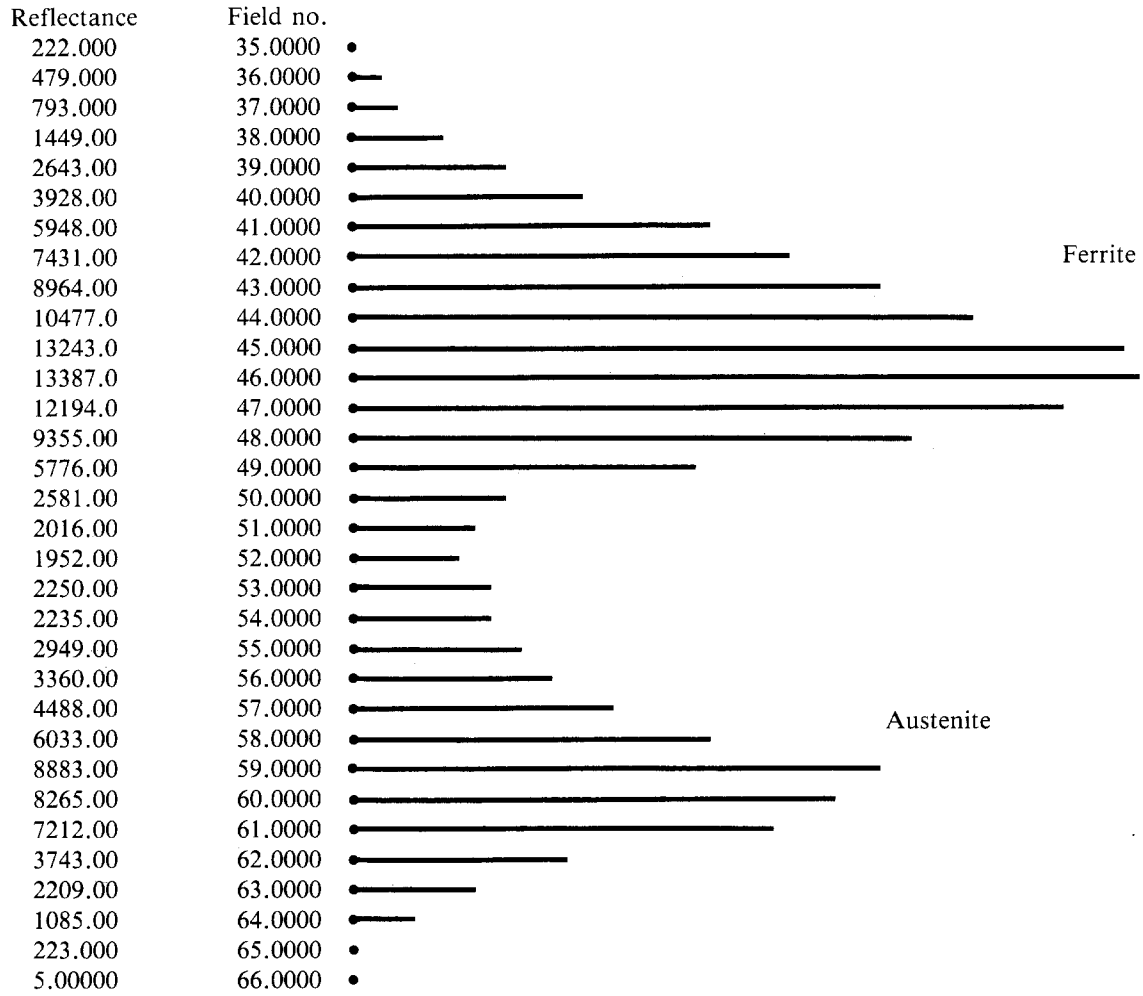

Figure 1 Histogram of reflectance values for ferrite and austenite from image analyser.

the measurement of the volume fraction of ferrite. Since the two phases in a duplex stainless steel are electrochemically different, the potential applied to the specimen during etching is of great importance. The objective is to select a potential where the difference in the reactivity of the phases is the greatest. This would then best ensure film formation of different thickness on the two phases, which would result in a sharp reflectance difference for quantitative phase content measurements.

This paper describes the potentiostatic etching of duplex stainless steels with different chemical compositions in a concentrated (10 N) sodium hydroxide solution. Potential conditions for film formation can easily be determined by potentiodynamic scans. These scans clearly indicate the passive regions where film formation occurs when the specimens are polarized in solutions. This approach formed an important part of the current investigation, which aimed to determine which etching potential gives the best results for a particular alloy, and the way in which this potential is related to the potentiodynamic response of an alloy in the same solution. Another goal was to establish the influence that different alloying elements have on these potentials and how this relates to the most suitable etching potential. This would yield quantitative

TABLE I Compositions of the different alloys used

	Composition (wt %)									
Alloy	Fe	Cr	Ni	Mo	Mn	Cu	N	Si	O	C
M 1902	Bal	19.2	2.10	2.20	4.63	3.20	0.09	0.55	0.02	0.040
M 2202	Bal	21.8	2.20	3.05	4.41	3.02	0.14	0.46	0.02	0.045
SAF2205 (a.c.)[a]	Bal	22.0	5.57	3.00	1.46	0.06	0.14	0.32	–	–
SAF2205	Bal	22.0	5.50	3.00	2.00	–	0.14	1.00	–	0.030
M 2209	Bal	22.0	9.07	2.81	0.10	–	0.006	0.07	0.02	0.030
M 2914	Bal	28.5	14.4	2.70	0.10	–	0.002	0.02	0.08	0.010
M 3518	Bal	34.7	18.6	2.72	0.01	–	0.005	0.03	0.07	0.020

[a] As cast.

data that would scientifically describe and characterize a field that is often regarded as an art, rather than a very useful and important discipline.

2. Experimental procedure

Longitudinal specimens of different cast and wrought experimental and commercial duplex stainless steels were used to investigate the effect of potentiostatic etching on the accuracy of phase delineation as a function of various etching parameters (e.g. potential, time, composition of alloy). It is generally accepted [9] that sample preparation is of the utmost importance if reliable and reproducible results are to be obtained. Extreme cleanliness during polishing procedures is also essential.

In the current investigation, samples were prepared automatically from pre-grinding to a 1 μm diamond-paste finish. Care was taken to ensure that the surface of each specimen was kept wet after final polishing and before it was immersed in the etchant. This was accomplished by the rinsing of the surface with water and then with ethanol after a final polishing. The slightest contact with air at this stage leads to erroneous results, presumably because of slight oxidation (passivation) of the surface.

The apparatus used for potentiostatic etching consists of a potentiostat of simple design, and an electrolytic cell in which the specimen-holder assembly and the electrodes are mounted in a cradle. The specimen-holder assembly and the cradle are designed specifically so that the distance between the electrodes and the specimen is constant. The specimen is held against the window of the specimen-holder by an O-ring in order to prevent ingress of the electrolyte. This holder is screwed into the body of the assembly against another O-ring. Electrical contact is established via a spring, one end of which is in contact with a contact-plate in the body, while the other contacts the specimen through a hole drilled in the back of the Bakelite mounting. The spring contact allows specimens of different lengths to be used. The front of the holder fits into a slot machined in the cradle. In this arrangement, the specimen acted as an anode, while a commercially available platinum electrode was used as a counter-electrode. An ordinary saturated calomel electrode, which was used as a reference electrode, completed the apparatus. After etching, each specimen was rinsed with water and ethanol, and dried with compressed air.

The specimens used for tint-etching were also prepared to a 1 μm diamond-paste polish. Beraha's etchant [10] B1 was used to etch both samples. The etchant was prepared by the use of 100 ml stock solution consisting of 24 g of ammonium difluoride dissolved in a mixture of 1000 ml of distilled water and

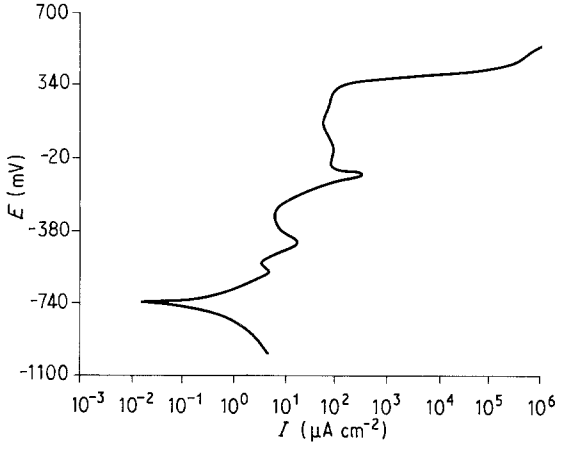

Figure 2 Potentiodynamic scan of M1902 in 10 N NaOH at 25 °C.

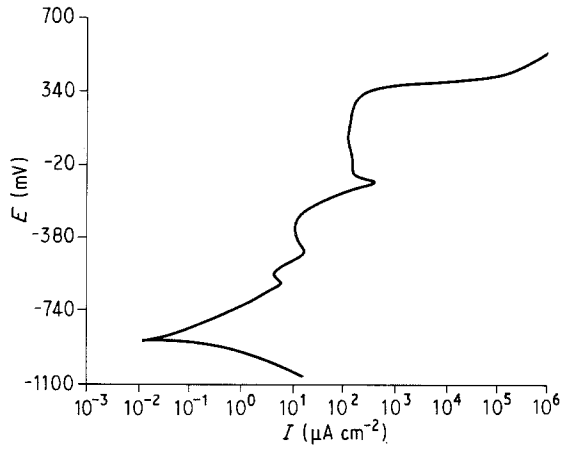

Figure 3 Potentiodynamic scan of M2202 in 10 N NaOH at 25 °C.

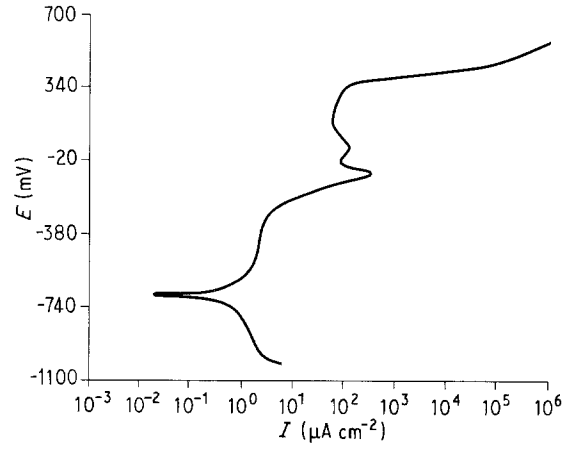

Figure 4 Potentiodynamic scan of SAF2205 in 10 N NaOH at 25 °C

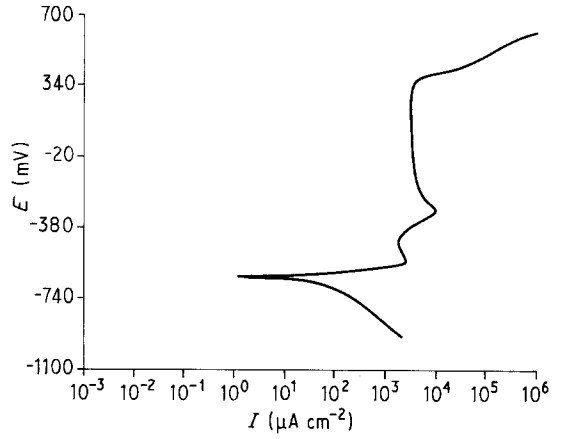

Figure 5 Potentiodynamic scan of SAF2205 (as cast) in 10 N NaOH at 25°C.

200 ml of concentrated hydrochloric acid. To this stock solution 1 g of potassium bisulphate was added. This solution is stable for about 2 h or until it becomes turbid. (Care should be taken to work only with plastic containers, since the dissolution of ammonium difluoride in a strong acid environment produces hydrofluoric acid). Immediately after they were polished on the 1 μm cloth, the samples were wet-etched by immersion in the solution for 5–10 s. At this stage the surfaces changed colour to a blue/grey type of colour.

The ferrite content was measured by use of a Cambridge Instruments Quantimet 10 image analyser. Twenty measurements were carried out on different areas of each sample, and were averaged to give the ferrite content. Sodium hydroxide etched the ferrite phase in the duplex stainless steels dark, while the austenite phase became a light colour. Photographs of the specimens were taken on an Olympus Vanox-T metallurgical microscope with halogen illumination. XRD spectra were recorded on a Siemens D500 X-ray diffractometer.

Potentiodynamic scans were recorded on a Princeton Applied Research model 273 potentiostat. All solutions were de-aerated for at least 45 min before any data were recorded. Specimens were held at − 900 mV for 5 min before data were collected, in order to reduce any surface oxide layer that might have been present. The experiments were conducted at 25 °C.

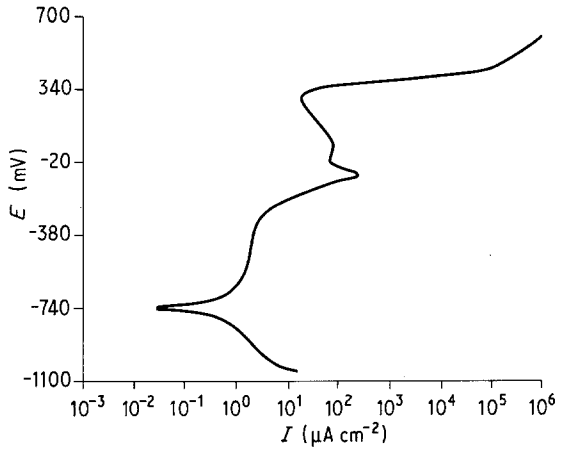

Figure 6 Potentiodynamic scan of M2209 in 10 N NaOH at 25°C.

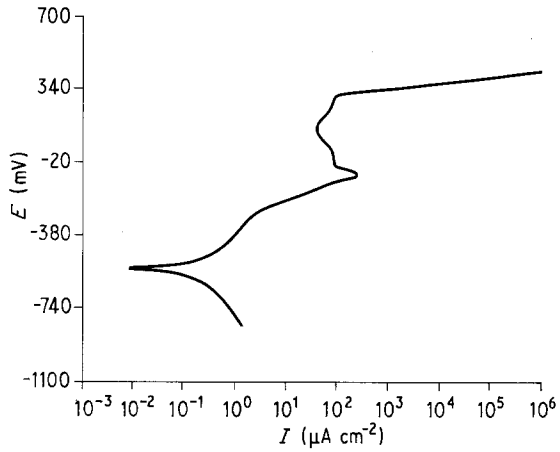

Figure 7 Potentiodynamic scan of M2914 in 10 N NaOH at 25°C.

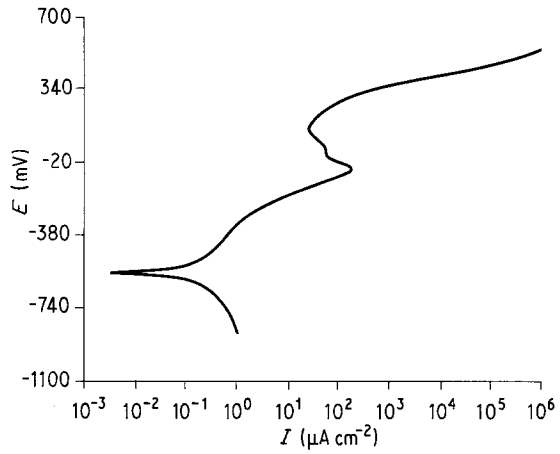

Figure 8 Potentiodynamic scan of M3518 in 10 N NaOH at 25 °C.

The compositions of the different alloys used in this investigation are summarized in Table I.

3. Results and discussion

Potentiodynamic scans, shown in Figs 2–8, were carried out in 10 N NaOH at 25 °C for each of the alloys used in the investigation, so that characteristic features could be established, such as the open-circuit (or corrosion) potential, the critical current density at passivation, the passivation range, the passivation potential, and the transpassive or breakaway potential at the end of the passivation range. A summary of

TABLE II Electrochemical parameters

Alloy	E_{cor} (mV)	$E_{pass,1}$ (mV)	$E_{pass,2}$ (mV)	$E^{a}_{pass,3}$ (mV)	E^{b}_{trans} (mV)	i_{crit} (μA cm^{-2})	Passive range (mV)
M1902	− 737	− 591	− 435	− 101	319	266	420[c]
M2202	− 880	− 592	− 444	− 96	342	347	438[c]
SAF2205	− 687	− 67	–	–	357	297	424
SAF2205 (a.c.)	− 630	− 536	–	− 284	372	9225	656[c]
M2209	− 726	− 78	–	–	314	240	392
M2914	− 544	− 78			296	246	374
M3518	− 557	− 47	–	–	163	170	210

[a] Taken at the onset of the most prominent passive range.
[b] Taken at the end of the most prominent passive range.
[c] Defines the most prominent passive range.

TABLE III Etching time and potentials of the different duplex stainless steels investigated

Alloy	Figure	Position of potential	Potential (mV)	Time (s)	Remarks
M1902	9 a	Onset of transpassive region	600	30	Insufficient contrast for phase determinations
	9 b	In passive region	319	90	Poor contrast
M2202	10 a	Above transpassive region	800	30	Insufficient contrast for phase determinations
	10 b	In passive region	342	60	Very poor contrast
	10 c	Below prominent passive region	− 94	300	No contrast between phases
SAF2205	11 a	Above transpassive region	1600	15	Good contrast, showing ferrite, austenite and σ-phases
	11 b	At onset of transpassive region	357	240	Reasonable contrast, showing ferrite, austenite and σ-phases
	12 a	In passive region	49	270	Poor contrast, showing ferrite, austenite and σ-phases
	12 b	At onset of passive region	− 67	270	Poor contrast, between ferrite, austenite and σ-phases still visible
SAF2205 (a.c.)	13 a	Above transpassive region	1600	30	Good contrast, showing ferrite, austenite phases
	13 b	In transpassive region	700	60	Reasonable contrast between phases
M2209	14 a	In transpassive region	500	15	Good contrast, showing ferrite and austenite phases
	14 b	At onset of transpassive region	350	45	As above
	15 a	High in passive region	314	120	Poor contrast between phases, but still reasonable
	15 b	Low in passive region	272	180	As above
M2914	16 a	In transpassive region	500	10	Good contrast between phases
	16 b	High in passive region	296	30	Reasonable contrast
	16 c	Low in passive region	30	120	Very poor contrast
M3518	17 a	High in passive region	300	12	Good contrast between different phases
	17 b	Low in passive region	160	150	As above
	18	Below passive region	− 47	60	Very poor contrast

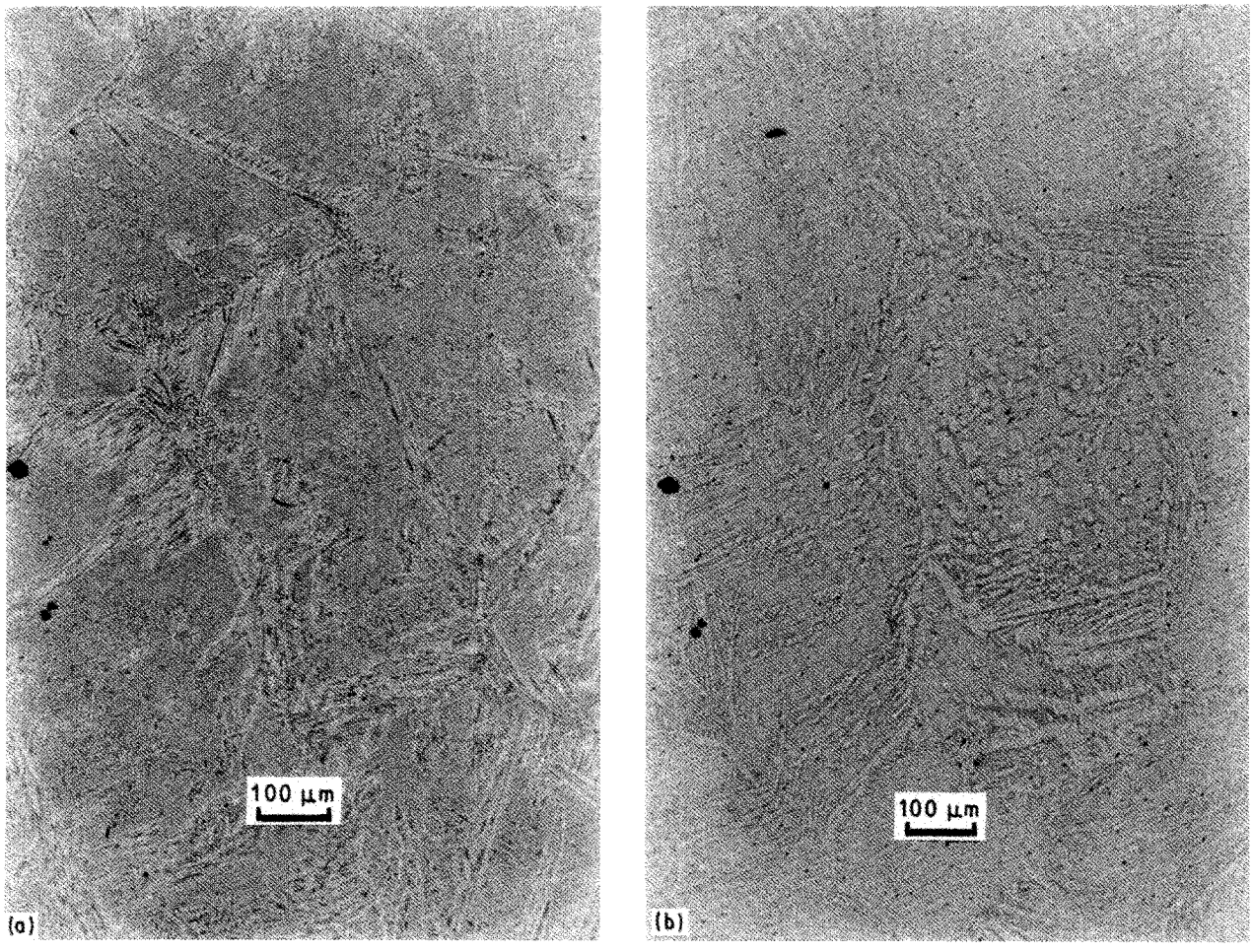

Figure 9 Microstructure of alloy M1902, etched in 10 N NaOH at 25 °C: (a) at 600 mV for 30 s, (b) at 319 mV for 90 s.

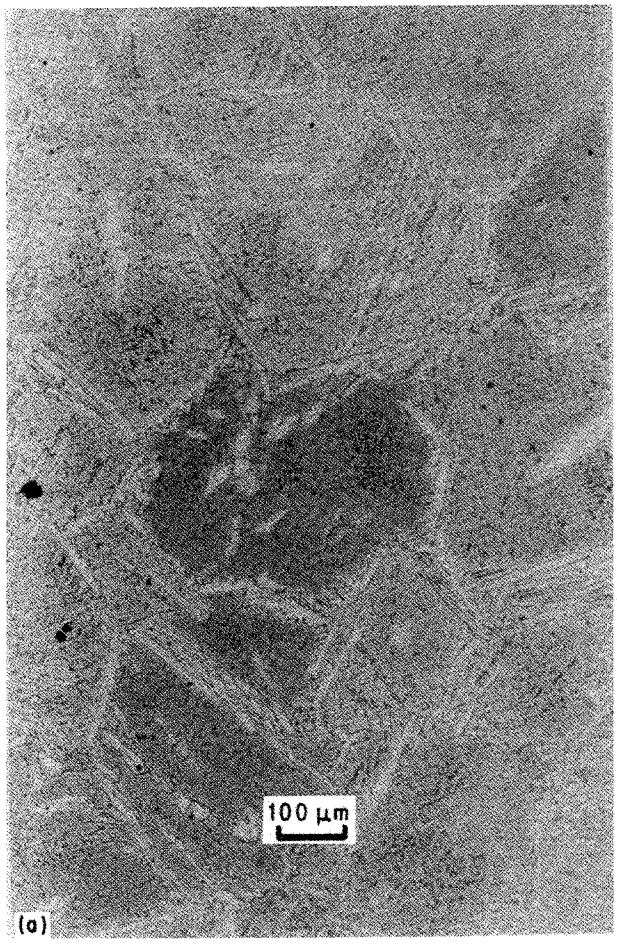

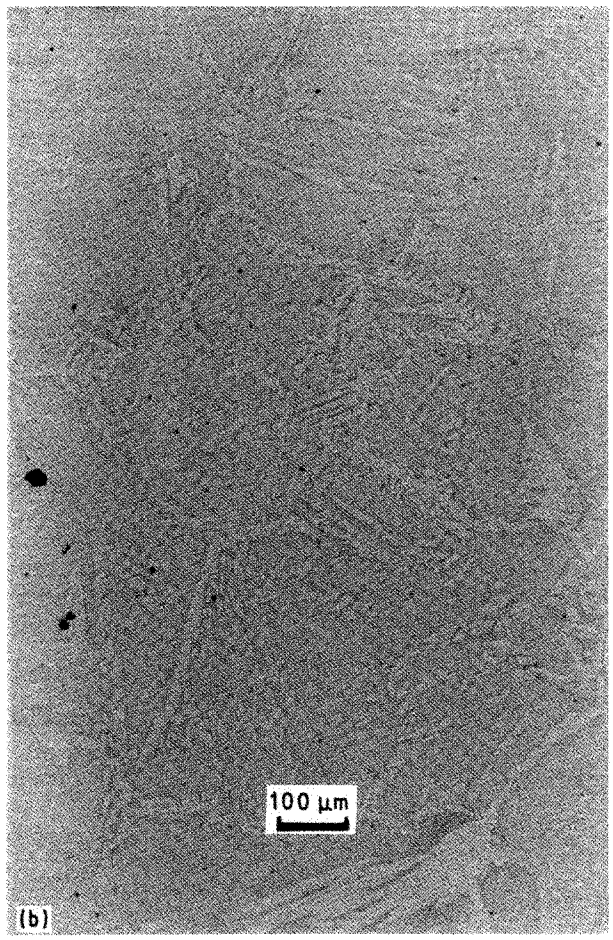

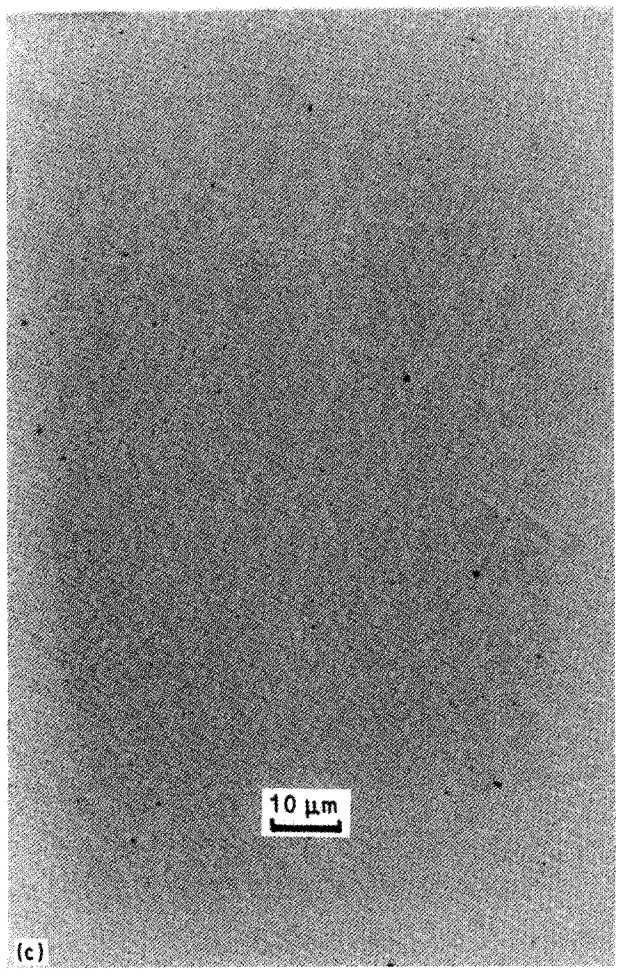

Figure 10 Microstructure of alloy M2202 etched at (a) 800 mV for 30 s, (b) 342 mV for 60 s, (c) − 94 mV for 300 s. Ferrite grey and dark grey, austenite white.

these electrochemical parameters is given in Table II. The values summarized here were used to identify the different potentials at which the etching procedure could be investigated.

The samples were etched at the voltages recorded at the onset of the passive region, those in the passive potential range, those at the end of the passive range where transpassivity started, and also voltages above this range, as shown in Table III. The etching time was varied until the maximum contrast was obtained. The results are shown in Figs 9–18.

The response of a particular phase to etching may vary considerably, depending on which constituents are present in the alloy. Good examples are the alloys M1902 and M2202 which contain 3.20 and 3.02 % copper, respectively. It was not possible to obtain sufficient contrast between ferrite and austenite at any potential chosen from the potentiodynamic scan conducted in 10 N NaOH. For the purpose of comparison, the austenite and ferrite phase compositions of all alloys containing 22 % Cr that were investigated are summarized in Table IV. Sufficient contrast could not be obtained even at 1600 mV, whereas other 22 % Cr duplex alloys normally gave an excellent etch. It has been observed previously with similar alloys [11]

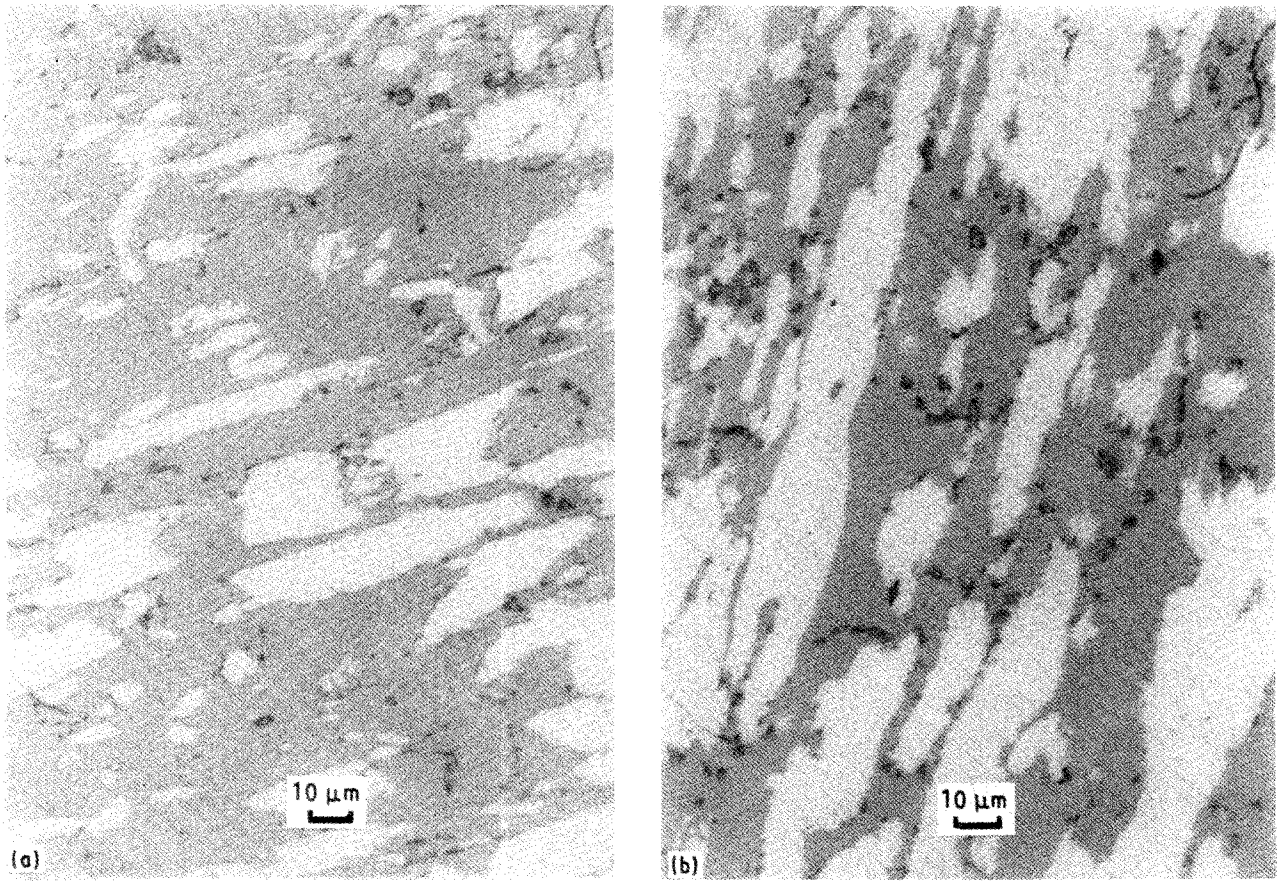

Figure 11 Microstructure of alloy SAF2205 etched at (a) 1600 mV for 15 s, and (b) 357 mV for 240 s. Ferrite grey, austenite white and σ-phase now dark grey.

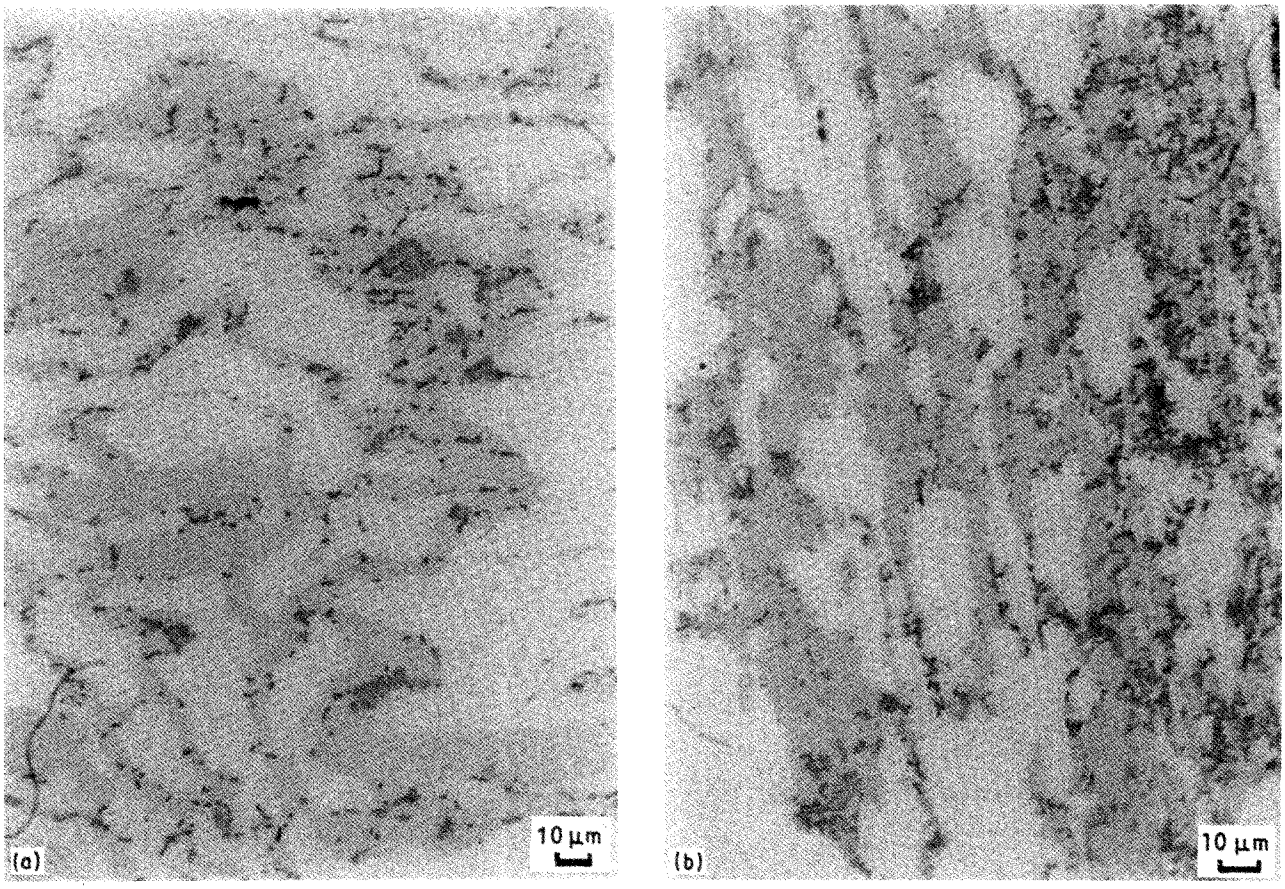

Figure 12 Microstructure of alloy SAF2205 etched at (a) 49 mV and (b) − 67 mV for 270 s. Ferrite medium grey, σ-phase dark grey and austenite light grey.

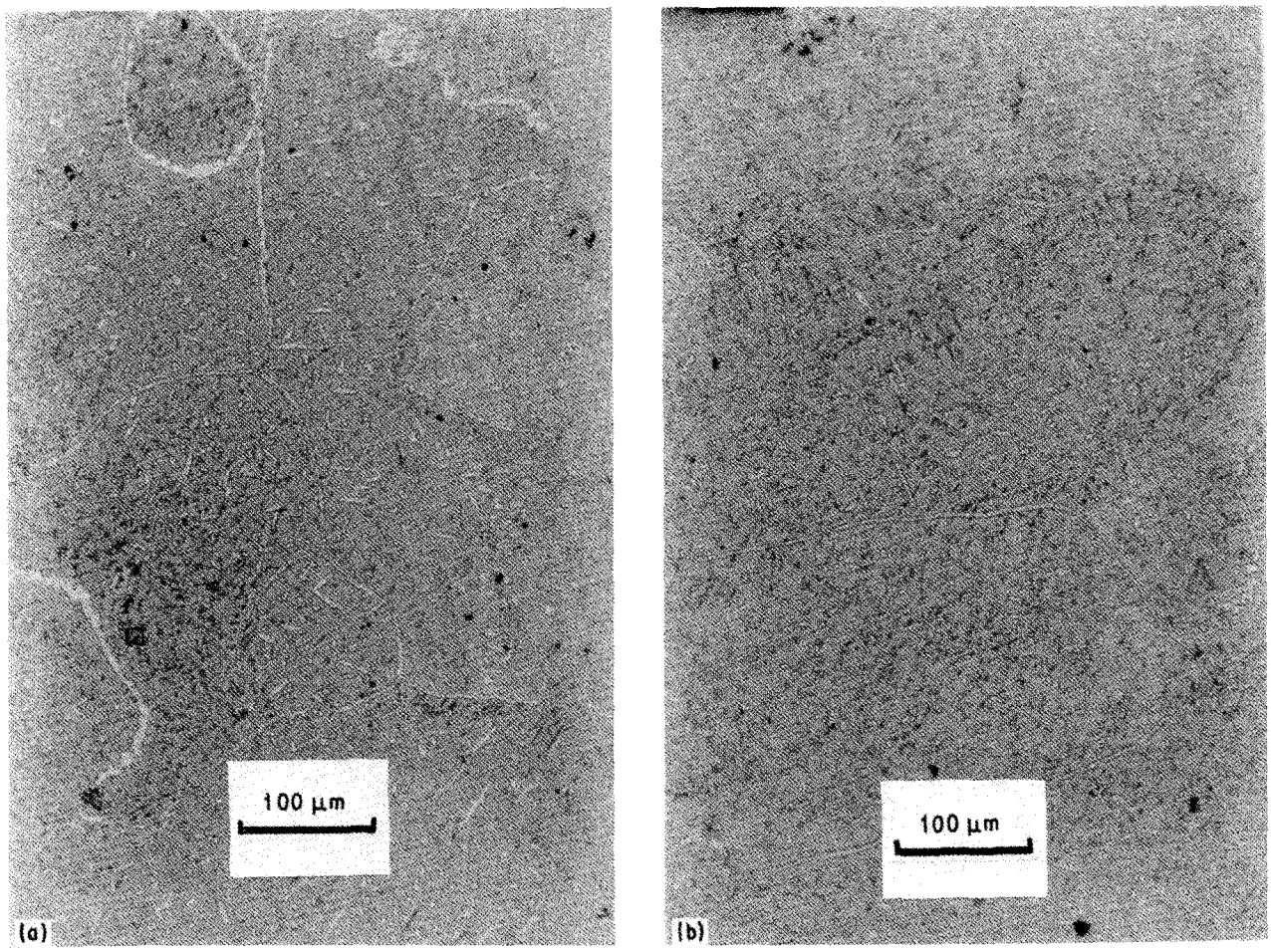

Figure 13 Microstructure of alloy SAF2205 (as cast) etched at (a) 1600 mV for 30 s and (b) 700 mV for 60 s. Ferrite grey, austenite white.

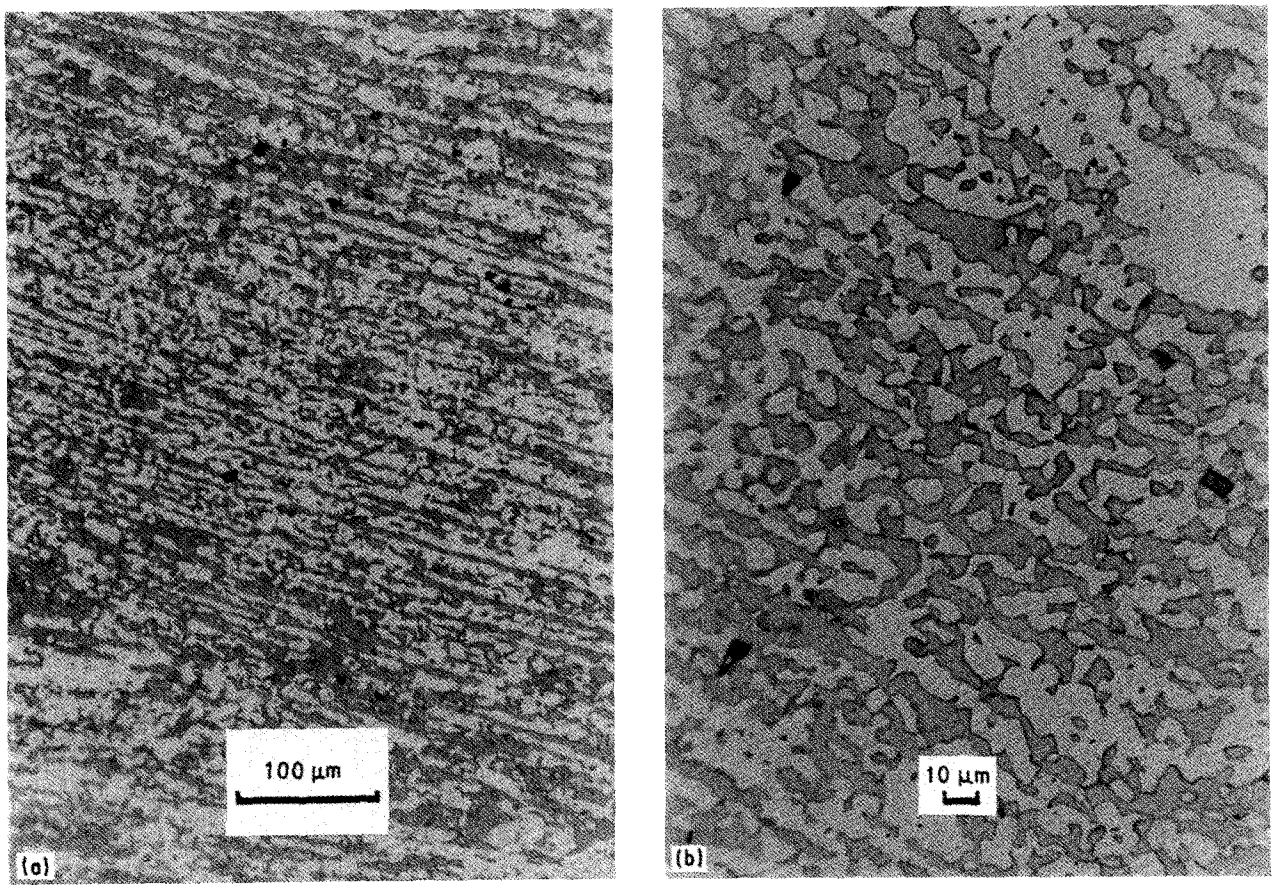

Figure 14 Microstructure of alloy M2209 etched at (a) 500 mV for 15 s and (b) 350 mV for 45 s. Ferrite dark, austenite light.

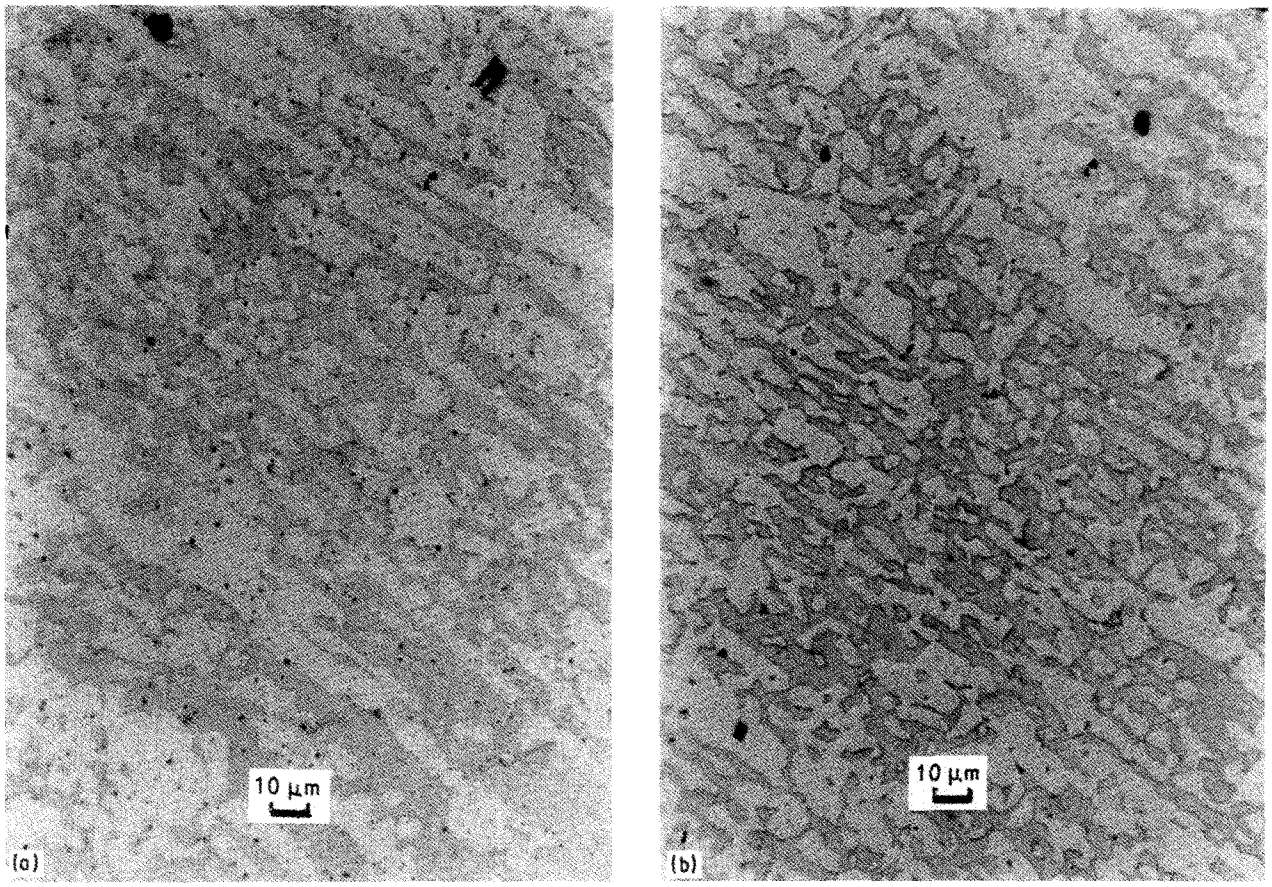

Figure 15 Microstructure of alloy M2209 etched at (a) 314 mV for 120 s and (b) 272 mV for 180 s. Ferrite dark, austenite light.

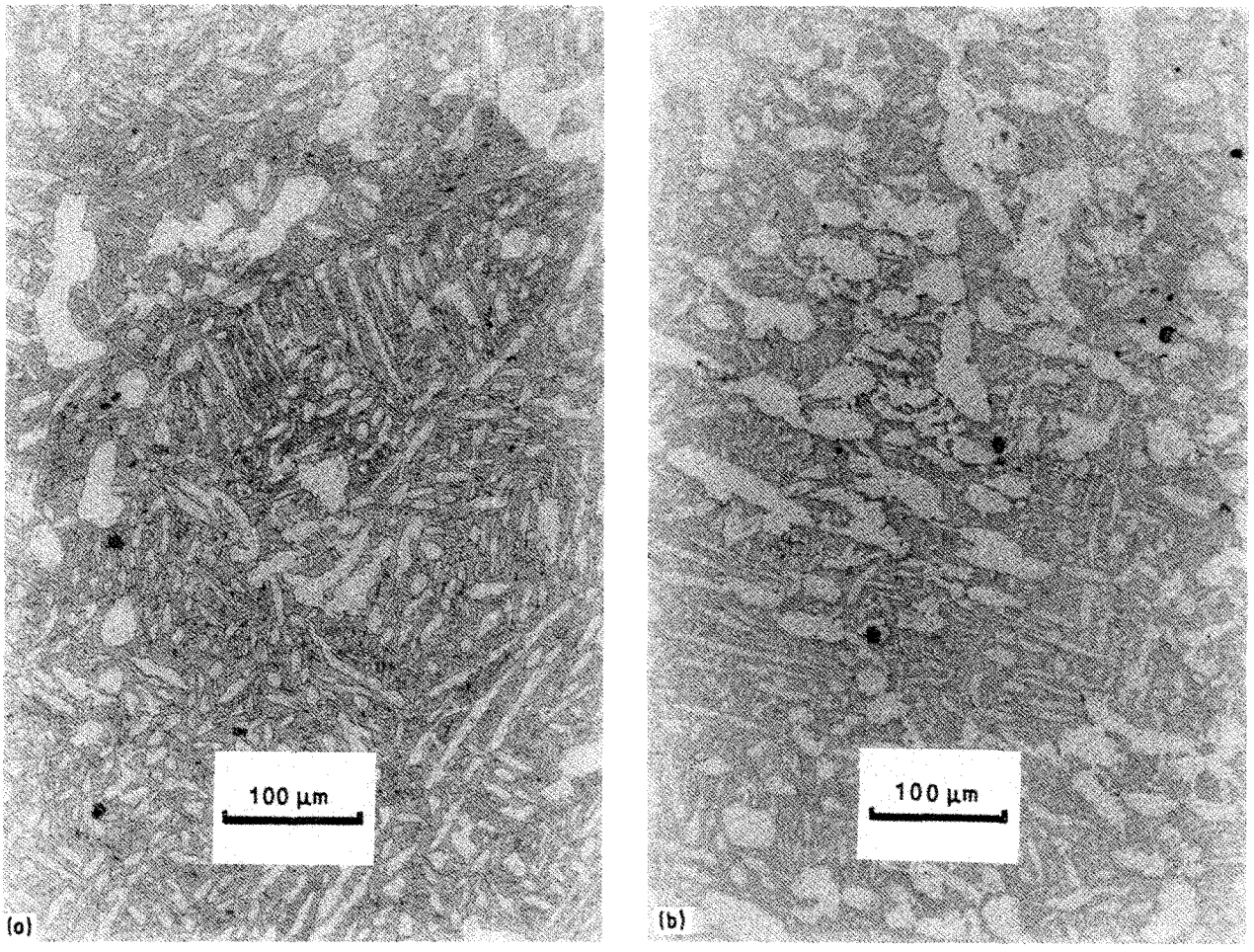

Figure 16 Microstructure of alloy M2914: (a) etched at 500 mV for 10 s (ferrite dark, austenite light); (b) etched at 296 mV for 30 s (ferrite dark, austenite light); (c) etched at 30 mV for 120 s (ferrite slightly darker than austenite).

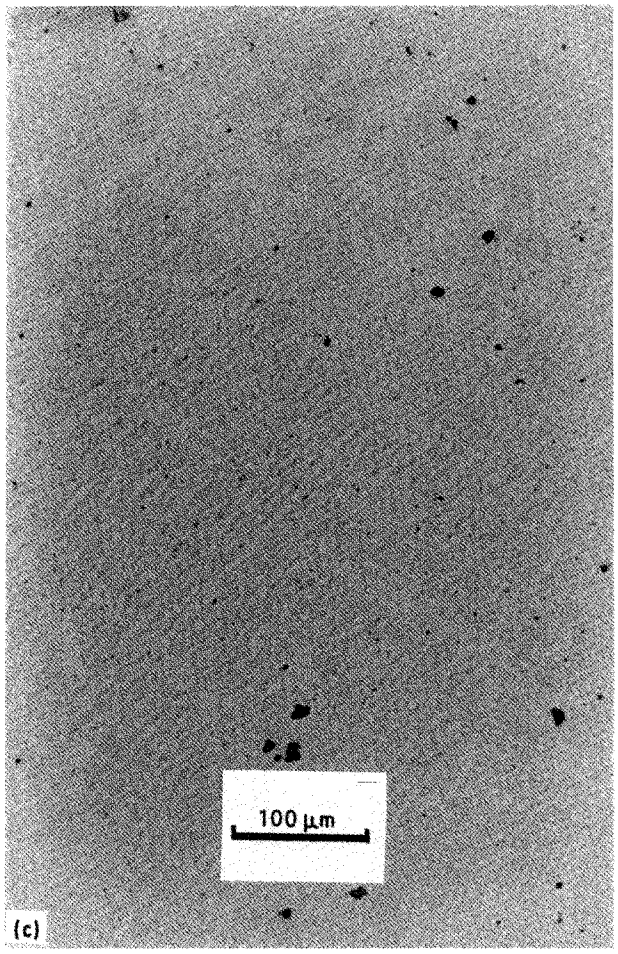

Figure 16 continued.

that it is easier to obtain a good contrast with low-copper alloys.

As expected, the chromium content of the alloy is also an important factor in determining the contrast between ferrite and austenite. At lower chromium contents it is more difficult to obtain good contrast between the phases. It was also found that at higher chromium contents a lower potential is required for etching, and the contrast is better. A comparison of the chromium content of each phase of all the alloys and the best etching potential for each alloy is given in Table V.

The use of lower potentials on the potentiodynamic scan did not prove advantageous for image analysis. The different phases can be differentiated after etching at lower potentials, but the contrast is insufficient for quantitative purposes. It was also observed that when lower potentials are used the current tends to fluctuate with increased etching time, and therefore the accuracy and reproducibility are questionable. It was found that in most cases the best contrast could be obtained when a potential in the transpassive region, or an even higher value, was used. None of the alloys investigated yielded sufficient contrast for quantitative differentiation between the different phases at potential values in the passive potential range.

Micrographs showing the microstructures of alloys M1902 and M2202, etched in Beraha's tint-etch, are depicted in Figs 19 and 20, respectively. The ferrite phase in each alloy was stained a deep brownish/blue shade that gave excellent constant colour contrast and

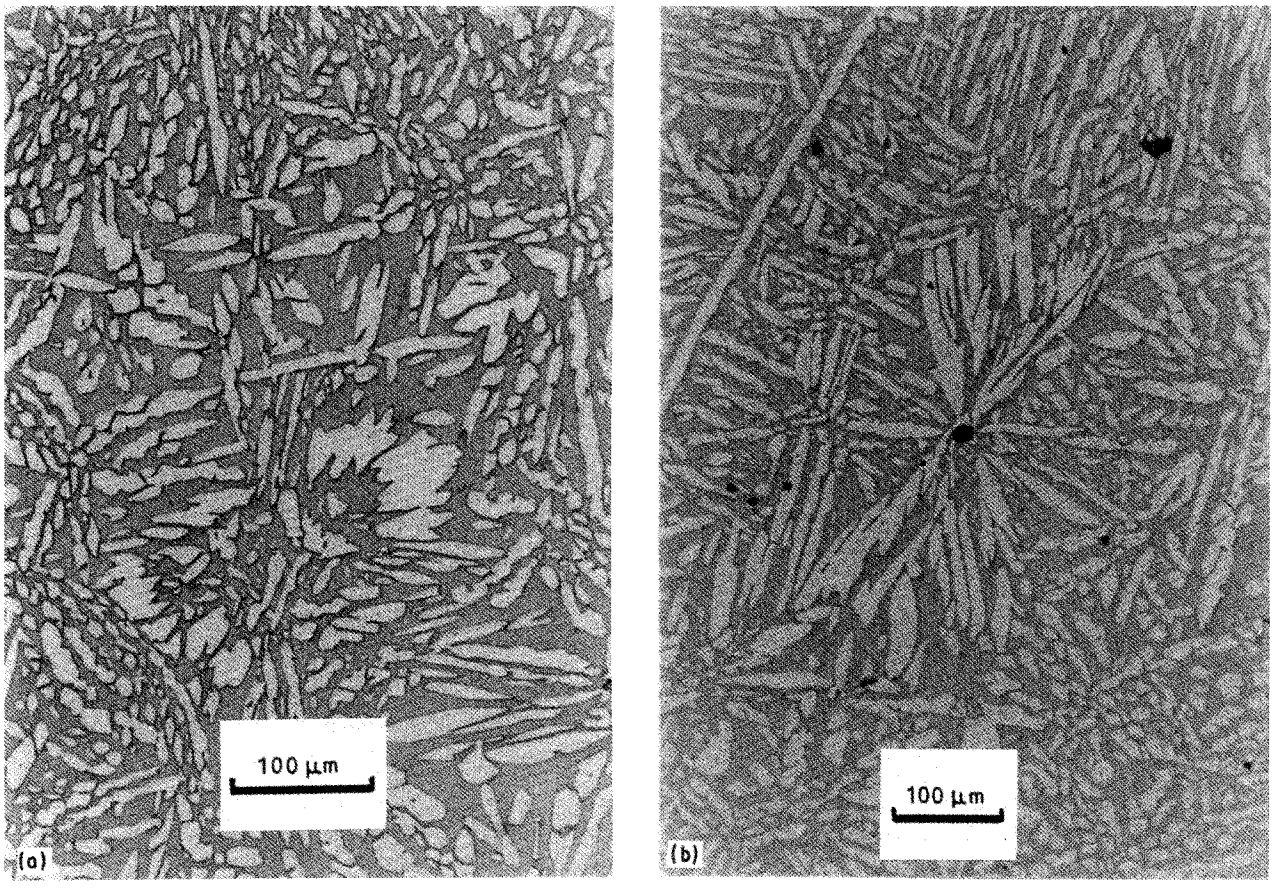

Figure 17 Microstructure of alloy M3518 etched at (a) 300 mV for 12 s and (b) 160 mV for 150 s. Ferrite dark, austenite light.

TABLE IV Austenite and ferrite phase compositions (wt %) of duplex alloys containing 22 % Cr

Alloy	Austenite				Ferrite			
	Cr	Ni	Mo	Cu	Cr	Ni	Mo	Cu
M2202	21.81	2.14	2.49	3.05	22.50	1.99	3.09	2.75
SAF2205	21.33	6.59	2.21	–	25.45	3.46	3.80	–
SAF2205 (a.c.)	17.51	7.06	2.07	–	23.3	4.56	3.25	–
M2209	19.59	10.61	2.51	–	25.35	6.15	4.16	–

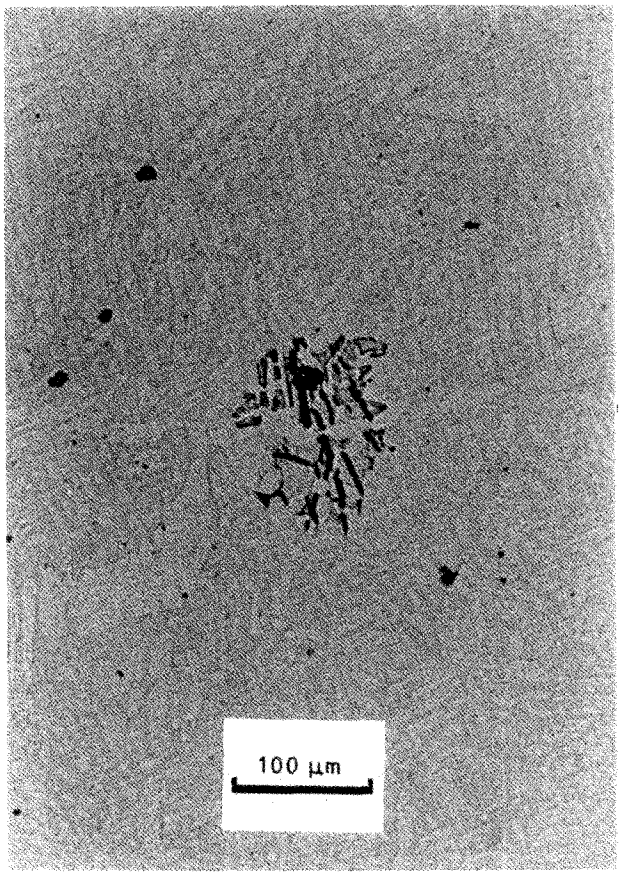

Figure 18 Microstructure of alloy M3518 etched at − 47 mV for 60 s. Ferrite slightly darker than austenite; some σ-phase appears in high relief.

TABLE V Chromium content of each phase of every duplex alloy investigated together with the most suitable etching potential

Alloy	Cr content (wt %)		Best etching potential (mV versus SCE)
	Austenite	Ferrite	
M1902	19.12	20.12	–
M2202	21.81	22.50	–
SAF2205	21.33	25.45	1600
SAF2205 (a.c.)	17.51	23.30	1600
M2209	19.59	25.35	≥ 500
M2914	24.02	34.87	≥ 500
M3518	27.56	41.26	≥ 300

boundary delineation for phase determinations. Both samples were also analysed by the use of XRD in order to determine the austenite phase content. The XRD spectra obtained are shown in Figs 21 and 22. Table VI summarizes the results of the phase determinations by image analysis (IA) and XRD for both alloys.

Figure 19 Microstructure of alloy M1902 in Beraha's No. 1 tint-etch solution. Austenite light, ferrite dark.

It is immediately obvious that the results of the two techniques are completely different for the M1902 alloy, while there is a reasonably good agreement within the limits of experimental error for the M2202 alloy. This discrepancy is caused by the large deviation (45.5 %) from the nominal ratio between the 3 1 1 and 2 2 0 austenite reflections (1.56 as compared with the ideal value of 1.07) used in the calculation of the austenite content of the sample. This large deviation indicates a strong preferred orientation of austenite grains in the sample, whereas a random distribution is required for accurate analysis. Another reason for the poor agreement between the IA and XRD results could be the very small size of the sample. However, the reasonably good agreement of the results for the M2202 alloy indicates that the results of the image analysis can be accepted as an accurate estimation of the phase content of both alloy samples.

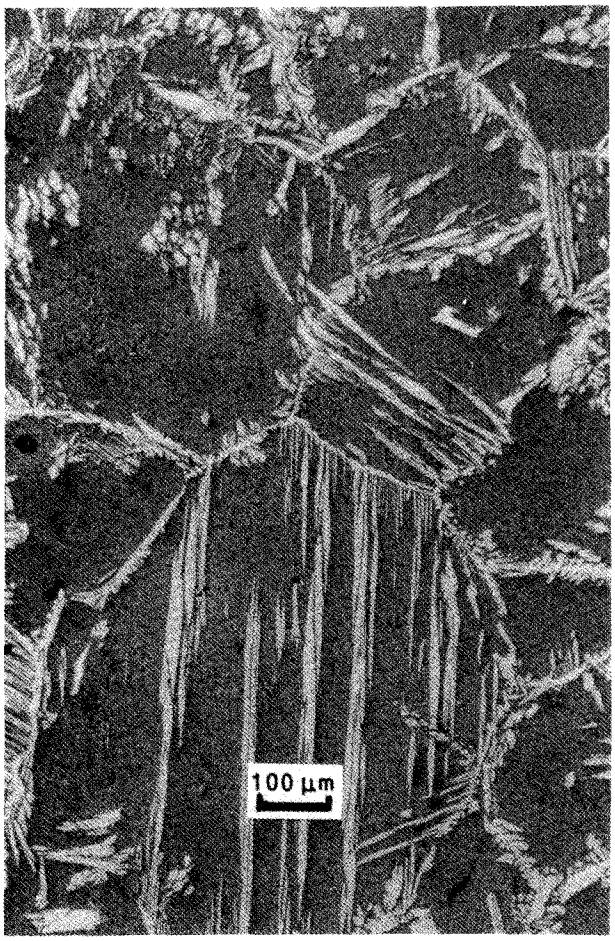

Figure 20 Microstructure of alloy M2202 etched in Beraha's No. 1 tint-etch solution. Austenite light, ferrite dark.

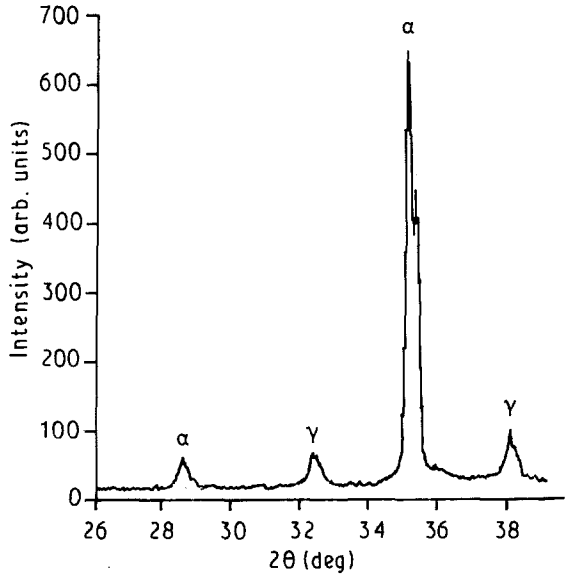

Figure 21 XRD spectrum of alloy M1902 showing the α and γ peaks used to calculate the austenite content.

4. Conclusions

The results of the investigation can be summarized as follows.

1. It was found that the best results are obtained with etching potentials substantially higher than those normally reached in the transpassive range of each alloy. No clear relationship could be established between the most suitable etching potential and the potentiodynamic response of the alloys, especially at values in the passive potential range. Only the duplex alloy containing 35 % Cr showed a satisfactory etch at its breakaway potential at the onset of the transpassive area.

2. In the case of duplex stainless steels containing significant levels of copper, it was difficult to obtain sufficient contrast by potentiostatic etching in the NaOH solution for the phases to be determined quantitatively. Previous work in these laboratories [11] proved that high-manganese duplex alloys with very low or no copper content can be suitably etched for quantitative phase determinations in a 10 N NaOH solution. It was found that when a tint-etch was used, sufficient contrast could be obtained for accurate phase determinations.

3. In the copper-free duplex alloys, the most suitable etching potentials and etching times decrease with increasing chromium content.

4. At lower etching potentials and longer etching times, current oscillations occur. It is therefore advisable to etch at the highest possible etching potential for the shortest practical time, in order to obtain good results.

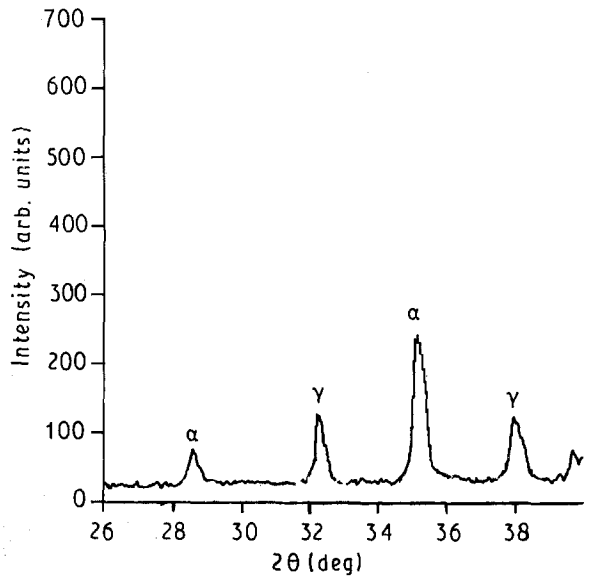

Figure 22 XRD spectrum of alloy M2202 showing the α and γ peaks used to calculate the austenite content.

TABLE VI Results of phase determinations by IA and XRD

Alloy	IA		XRD	
	α (%)	γ (%)	α (%)	γ (%)
M1902	67.4 ± 5.3	32.6	80.9	19.1
M2202	62.1 ± 4.9	37.9	55.9	44.1

References

1. J. H. DALTON, M. SMITH and P. DE VISSER, in Proceedings of Stainless Steel '87 Conference, University of York, UK, 1987 (Institute of Metals, London, 1988) p. 568.

2. E. E. STANSBURY, in "Applied Metallography", edited by G. F. Vander Voort (Van Nostrand Reinhold, New York, 1986), pp. 21–39.
3. D. E. NELSON, W. A. BAESLACK and J. C. LIPPOLD, *Metallography* **18** (1985) 215.
4. G. F. VANDER VOORT, *J. Minerals. Metals & Materials Soc.* **41** (1989) 6.
5. T. A. DEBOLD, *ibid.* **41** (1989) 12.
6. D. J. KOTECKI, *Welding Res. Suppl.* (1986) 273s.
7. P. de VISSER, Unpublished Results (1988)
8. J. H. POTGIETER and M. B. CORTIE, *Mater. Characteriz.* **26** (1991) 155–165
9. G. F. VANDER VOORT, in "Microstructural Science", Vol. 9, edited by, G. Petzow, R. Paris, E. D. Albiecht and J. L. McCall (Elsevier–North-Holland, New York, 1981) pp. 137–154.
10. E. WECK and L. LEISTNER, "Metallographic instructions for colour etching by immersion. Part II: Beraha colour etchants and their different variants", Deutsher Verlag fur Schweisstechnik, Dusseldorf, 1982.
11. S. NANA, Unpublished Results (1989).

Received 12 March
and accepted 1 July 1991